Proceedings of the ASME 2016 35th International Conference on Ocean, Offshore and Arctic Engineering
OMAE2016
June 19-24, , Busan, South Korea

OMAE2016-55066

SHELTERING THE SHORE VIA NEARSHORE OBLIQUE SEABED BARS

Louis-Alexander Couston
Department of Mechanical Engineering
University of California Berkeley
Berkeley, California 94720
Email:louisalexandre.couston@berkeley.edu

Mir Abbas Jalali
Department of Astronomy
University of California Berkeley
Berkeley, California 94720
Email:mjalali@berkeley.edu

Mohammad-Reza Alam
Department of Astronomy
University of California Berkeley
Berkeley, California 94720
Email:reza.alam@berkeley.edu

ABSTRACT

Periodic seabed undulations, such as nearshore sandbars, are known to reflect incoming surface waves of twice the wavelength by the so-called Bragg resonance mechanism. In view of this property, longshore seabed-mounted bars were proposed long ago as a means of coastal protection against the high momentum of incident oceanic waves. Many theoretical, computational, experimental and field measurements were conducted to understand their effectiveness in shielding the shore. The idea, nevertheless, proved impractical when Yu and Mei (JFM 2000, [1]) showed that due to an inevitable finite reflection from the shoreline, energy can get trapped in the area between the shoreline and the patch of bars eventually resulting in a much higher wave energy flux impinging the shoreline. Here we propose an arrangement of oblique bars that shelters the shore by diverting, rather than reflecting, shore-normal incident waves to the shore-parallel direction. A protected buffer zone is thus created at the shoreline. We show that this novel arrangement can very efficiently shelter the shore, is almost insensitive to the distance between the bottom corrugations and the shoreline, is relatively robust against frequency detuning, and will discuss that it can be designed to protect the shore against almost the entire broadband spectrum of incident waves.

INTRODUCTION

The reflection of water waves by periodic corrugations on the seabed of half the surface wavelength has been investigated extensively owing to its importance in the formation of nearshore sandbars and the evolution of oceanic wave-field in littoral zones [2–6]. The phenomenon is sometimes referred to as *Bragg reflection or resonance* due to its similarity with the selected reflection of x-rays from the surface of a crystal in solid state physics [7]. In contrast to random scattering by a general irregular medium (e.g. [8, 9]), Bragg reflection is a coherent reflection by a periodic medium that satisfies the *Bragg resonance* condition.

Bragg resonance of water waves was first formulated for a weak reflection of monochromatic surface waves [10], whose results were verified experimentally [11]. The theory was shortly after extended [12, 13] to include longer time and stronger interactions. In particular, multiple scales analysis was applied to predict the variations of both the incident and reflected waves over the patch while keeping the overall energy conserved [13]. Similar results can be obtained through the mild slope approximation [14, 15].

The resonance condition $k_b = 2k$ [10], in which k_b denotes the seabed undulations wavenumber and k the surface wavenumber, is a special case of a more general Bragg condition that can be obtained using perturbation analysis with multi-modal bottom topography [16]. At the second order in perturbation analysis the classical Class I Bragg resonance is obtained which is due to triadic interactions between two surface waves and one bottom component [2, 11, 17–19]. At the third order, Class II occurs which involves quartic interactions between two surface waves and two bottom components [16, 20], and also the class III, another quartic interaction, this time between three surface waves and one bottom component [16, 21].

Longshore seabed-mounted bars were investigated exten-

sively as a means of coastal protection against the high momentum of incident oceanic waves [3, 22, 23]. Many theoretical, computational, experimental and field measurements were conducted to understand their effectiveness and limitations in shielding the shoreline. The progress was almost halted when [1, 24], based on earlier observations of [25], showed that while in theory Bragg reflection reflects part of the incident wave energy, due to the inevitable finite reflection from the shoreline, energy can get trapped in the area between the coast and the patch of bars, eventually resulting in a much higher wave energy flux impinging on the shoreline compared to when bars do not exist and the seafloor if perfectly flat [26]. Physically speaking what happens is that the part of energy reflected from the shoreline is again reflected back by the bars and as a result energy (over time) gets accumulated in the area between the patch of bars and the shoreline.

Here, we show that an approach based on oblique Bragg resonance can provide a viable alternative for shore protection by seabed bars. Specifically, we consider an arrangement of seabed bars that diverts normal-to-the-shore incident wave rays to parallel-to-the-shore reflected waves (c.f. e.g. [27]). We show, via perturbation analysis and numerical experiments, that this arrangement is very efficient in protecting the shore, and that it is insensitive to the shoreline-patch distance.

Sheltering the coastline by an array of seabed corrugations, unlike breakwaters, gradually diverts the incoming wave energy while posing much less stress on the seabed. It is more reliable (no sudden breakdown), cost effective (no major foundation needed), and environmentally friendly. The proposed idea may also be used to protect important nearshore infrastructures in shallow waters such as offshore wind farms that are susceptible and vulnerable to cyclic wave loads.

1 PROBLEM FORMULATION

Consider the problem of waves propagation on the surface of a homogeneous ocean of mean depth h. We define a Cartesian coordinate system with the x,y axes on the mean free surface, and the z axis positive upward. We assume that the fluid flow under consideration is inviscid, incompressible and irrotational such that potential flow theory applies, and hence the velocity vector $\vec{\mathbf{v}}$ can be expressed as the gradient of a scalar function ϕ (velocity potential), i.e., $\vec{\mathbf{v}} = \nabla\phi$. If we denote surface elevation, measured from the mean water surface, by $\eta(x,y,t)$ and the height of bottom corrugations, measured from the mean bottom (i.e. $z=-h$), by $\zeta(x,y,t)$, then the governing equations (continuity in the fluid domain and boundary conditions) read

$$\nabla^2\Phi = 0, \qquad -h+\zeta(x,y) \le z \le \eta(x,y,t), \quad \text{(1a)}$$

$$\Phi_{tt} + g\Phi_z + 2\nabla\Phi\cdot\nabla\Phi_t + \frac{1}{2}\nabla\Phi\cdot\nabla(\nabla\Phi\cdot\nabla\Phi) = 0, \qquad z=\eta(x,y,t), \quad \text{(1b)}$$

$$\Phi_z = \nabla_h\zeta\cdot\nabla_h\Phi, \qquad z=-h+\zeta(x,y), \quad \text{(1c)}$$

where $\nabla_h = (\partial_x, \partial_y)$ is the two-dimensional gradient operator. If the governing equation (1) is solved for $\phi(\mathbf{x},t)$, then the free-surface elevation $\eta(\mathbf{x},t)$ is obtained from the free-surface kinematic boundary condition:

$$\eta = -\frac{1}{g}(\Phi_t + \frac{1}{2}\nabla\Phi\cdot\nabla\Phi), \qquad z=\eta(x,y,t). \quad \text{(2)}$$

Under the assumption of small surface wave slope and small bottom corrugation slope (i.e. $\nabla_h\eta, \nabla_h\zeta = \mathscr{O}(\varepsilon) \ll 1$) a perturbation solution can be sought by expanding the velocity potential and free-surface elevation in perturbation series:

$$\Phi = \phi_1 + \phi_2 + \phi_3 + ..., \quad \text{(3a)}$$

$$\eta = \eta_1 + \eta_2 + \eta_3 + ..., \quad \text{(3b)}$$

where $(\phi_m, \eta_m) = \mathscr{O}(\varepsilon^m)$. Substituting (3) in (1) and collecting terms of the same order, we obtain a series of equations of the following form [6]

$$\nabla^2\phi_m = 0, \ \text{ in } \ -h \le z \le 0, \quad \text{(4a)}$$

$$\phi_{m,tt} + g\phi_{m,z} = \mathbf{F}^{(m)}(\phi_1,...,\phi_{m-1};\eta_1,...,\eta_{m-1}), \ \text{ on } \ z=0, \quad \text{(4b)}$$

$$\phi_{m,z} = \mathbf{B}^{(m)}(\phi_1,...,\phi_{m-1};\zeta), \ \text{ on } \ z=-h. \quad \text{(4c)}$$

At each order m, (4) is a linear partial differential equation for ϕ_m with the right hand side being a nonlinear function of the solutions to the lower order problems. As a result (4) can be solved sequentially starting from the leading order, i.e. the linear problem. The leading-order problem is unaffected by the bottom corrugations and its propagating wave solution can be written in the form

$$\phi_1 = A\frac{g}{2\omega}\frac{\cosh[k_1(z+h)]}{\cosh(k_1h)}e^{i(\mathbf{k_1}\cdot\mathbf{x}-\omega t)} + c.c., \quad \text{(5)}$$

$$\eta_1 = \frac{iA}{2}e^{i(\mathbf{k_1}\cdot\mathbf{x}-\omega t)} + c.c., \quad \text{(6)}$$

where $c.c.$ denotes complex conjugate, A is the wave amplitude, and $k_1 = |\mathbf{k_1}|$ is the magnitude of the wavenumber vector $\mathbf{k_1}$ that

together with the wave frequency ω have to satisfy the dispersion relation: $\mathscr{D}(\omega;k_1) \equiv \omega^2 - gk_1\tanh(k_1 h) = 0$.

At the second order (m=2), $\mathbf{B}^{(2)}$ becomes secular if the seabed corrugations have a Fourier component $\mathbf{k}_b$ such that $\mathscr{D}(\omega, |\mathbf{k}_1 \pm \mathbf{k}_b|)$=0 (note that at the second order $\mathbf{F}^{(2)}$ is never secular). In such a case, the solution to the second order problem includes a new wave with frequency ω and wavenumber $\mathbf{k}_2 = \mathbf{k}_1 \pm \mathbf{k}_b$ whose amplitude grows linearly with time. Because of this monotonic temporal growth of the second-order solution, this scenario is considered a resonant interaction, and since this interaction occurs between an incident wave and a periodic medium (i.e. the seabed undulations) it is called Bragg resonance, a name taken from a similar reflection mechanism in solid state physics [7].

Clearly this second-order solution is only valid for initial times, i.e. as long as the amplitude of the resonant wave $\mathbf{k}_2$ is small enough such that the perturbation expansion (3) is valid (i.e. $\phi_2 \ll \phi_1$). For longer times, multiple-scale analysis for an initial value problem shows that, while the amplitude of the resonant wave initially increases linearly with time, its rate of growth gradually slows down [13]. Eventually, this rate approaches zero when all the energy of the initial wave is transferred to the resonant wave and the amplitude of the initial wave is zero. At that time the direction of energy transfer reverses and energy flows back from the resonant wave to the initial wave. The modulation then continues. Bragg resonance at the second order involves one incident wave and one seabed component, and is called Class I Bragg resonance [6].

A classic example of Class I Bragg resonance occurs when the direction of propagation of the resonant wave is the exact opposite of that of the incident wave. Hence, the incident wave appears to be reflected back over the patch of bottom undulations (Bragg resonance is sometimes referred to as Bragg *reflection*). This reflection mechanism has motivated the use of artificial nearshore bars for shore protections: a few small amplitude seabed bars parallel to the shoreline can reflect back shoreward incoming waves and therefore protect the shoreline [3, 23]. The protection efficiency, defined as $1 - a_b/a$, where a_b and a are the wave amplitudes at the shoreline in the presence and in the absence of the bars, asymptotically approaches unity as the number of ripples (i.e. extent of the bars patch) increases [13, 16].

There is, however, a major issue in the realization of this protective mechanism: if the shore is not a perfectly absorbing beach and as a result reflects parts of the incident waves, which is in fact the case in most realistic settings, then the protection efficiency of the seabed bars are shown to be very sensitive to the distance between the shore and the patch of bars [1]. Specifically, for certain distances of the shoreline to the bar patch, the protection efficiency can become negative which means that the amplitude of the waves at the shoreline in the presence of (supposedly) protective bars are higher than in their absence. Physically speaking what happens is that the reflected waves from the shoreline are reflected back again (by the seabed bars) toward the shore, and therefore get trapped inside the area between the patch of bars and the shoreline. For some specific bar-patch to shoreline distances, these successive reflections interfere constructively to the point that wave elevation at the shoreline becomes (much) higher compared to when bars do not exits.

Here, we look for an arrangement of seabed bars that instead of reflecting waves back, that as was discussed may result in wave amplification, diverts incident wave rays sideways along a path parallel to the shoreline. In other words, desired seabed bars must redirect normal-to-the-shore incident wave rays to parallel-to-the-shore diverted (or reflected) waves. If an arrangement of bars with such a capability in diverting waves is found then there is no danger of having wave energy trapped between the shore and the patch of the bars.

The first candidate for diverting wave rays is the oblique Class I Bragg resonance. Class I Bragg resonance condition states that oblique seabed bars making $\pi/4$ radian angle with the incident waves result in a resonant wave perpendicular to the incident wave [21]. Unfortunately, the rate of energy transfer from the incident wave to the resonant wave in this scenario is exactly zero, making this case a degenerate resonance [3, 6]. With Class I resonance ruled out, we need to proceed in our perturbation analysis to the third order where the so-called Class II Bragg resonance can occur. Class II Bragg resonance states that if a free propagating surface wave with wavenumber $\mathbf{k}_1$ travels over a doubly sinusoidal seabed with components $\mathbf{k}_{b_1}, \mathbf{k}_{b_2}$, in such a way that $\mathscr{D}[\omega, \mathbf{k}_1 \pm (\mathbf{k}_{b_1} \pm \mathbf{k}_{b_2})]$=0, then a new wave with wavenumber $\mathbf{k}_3$= $\mathbf{k}_1 \pm (\mathbf{k}_{b_1} \pm \mathbf{k}_{b_2})$ is generated (resonated). Analysis of Class II Bragg resonance in the case that none of the pairs $(\mathbf{k}_1, \mathbf{k}_{b_1})$ and $(\mathbf{k}_1, \mathbf{k}_{b_2})$ form a Class I Bragg resonance is well known [6, 28]. It is, however, not difficult to see that the overall rate of energy transfer from the wave $\mathbf{k}_1$ to the resonant wave $\mathbf{k}_3$ is much higher if the incident wave $\mathbf{k}_1$ makes a Class I Bragg resonance with either $\mathbf{k}_{b_1}$ or $\mathbf{k}_{b_2}$ (see figure 1). This will be elaborated mathematically in the next section.

ENERGY TRANSFER RATE

Consider a Class II Bragg resonance between an incident wave $\mathbf{k}_1$ and a bottom topography made of the two sinusoidal corrugations $\mathbf{k}_{b_1}$ and $\mathbf{k}_{b_2}$. We select $\mathbf{k}_{b_1}$ and $\mathbf{k}_{b_2}$ such that $\mathbf{k}_1$ and $\mathbf{k}_{b_1}$ satisfy the Class I Bragg resonance condition, and such that the Class II resonant wave $\mathbf{k}_3$ is perpendicular to $\mathbf{k}_1$ (figure 1). The initial rate of energy exchange between the three waves can be found from perturbation theory. We first consider the second-order equations (c.f. equation (4))

$$\nabla^2\phi_2 = 0, \text{ in } -h \le z \le 0, \tag{7a}$$

$$\phi_{2tt} + g\phi_{2z} = \text{N.R.}, \text{ on } z = 0, \tag{7b}$$

$$\phi_{2z} = \nabla_h \cdot (\zeta \nabla_h \phi_1), \text{ on } z = -h, \tag{7c}$$

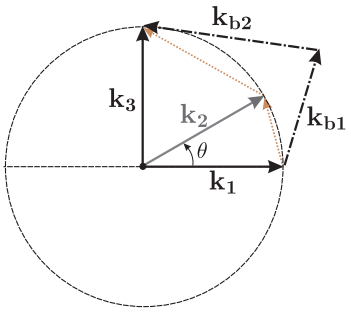

FIGURE 1: Geometric construction for Class II Bragg resonance condition: A free propagating wave $\mathbf{k}_1$ traveling over a doubly sinusoidal topography with wave numbers $\mathbf{k}_{b_1}, \mathbf{k}_{b_2}$ resonates a new wave $\mathbf{k}_3$ if $|\mathbf{k}_1| = |\mathbf{k}_1 + \mathbf{k}_{b_1} + \mathbf{k}_{b_2}|$ (i.e. if the vector $\mathbf{k}_1 + \mathbf{k}_{b_1} + \mathbf{k}_{b_2}$ ends up on the dashed circle). In this case the resonant wave wavenumber is $\mathbf{k}_3 = \mathbf{k}_1 + \mathbf{k}_{b_1} + \mathbf{k}_{b_2}$. Of particular interest in this manuscript is the special case of Class II when $\mathbf{k}_1$ and $\mathbf{k}_{b_1}$ satisfy the Class I Bragg resonance condition generating a free propagating intermediate wave $\mathbf{k}_2$. Energy eventually transfers to the resonant wave $\mathbf{k}_3$ via $\mathbf{k}_{b_2}$.

in which N.R. denotes non-resonant forcing terms. We consider the form of the bichromatic topography as

$$\zeta = \frac{d_1}{2}(e^{\mathbf{k}_{b1}\cdot\mathbf{x}} + e^{-\mathbf{k}_{b1}\cdot\mathbf{x}}) + \frac{d_2}{2}(e^{\mathbf{k}_{b2}\cdot\mathbf{x}} + e^{-\mathbf{k}_{b2}\cdot\mathbf{x}}), \tag{8}$$

where d_1, d_2 are real amplitudes. The solution to (7) is

$$\begin{aligned}\phi_2 =& \mathscr{K}_2^{\pm}(z)\mathrm{e}^{i(\mathbf{k}_1\pm\mathbf{k}_{b2})\cdot\mathbf{x}-i\omega t} + \mathscr{K}_1^{-}(z)\mathrm{e}^{i(\mathbf{k}_1-\mathbf{k}_{b1})\cdot\mathbf{x}-i\omega t}\\ &+ [\mathscr{D}(z) + t\mathscr{E}(z)]\,\mathrm{e}^{i(\mathbf{k}_2\cdot\mathbf{x}-\omega t)} + c.c.,\end{aligned} \tag{9}$$

where

$$\mathscr{K}_j^{\pm}(z) = -\frac{Agd_j\mathbf{k}_1\cdot(\mathbf{k}_1\pm\mathbf{k}_{bj})}{4|\mathbf{k}_1\pm\mathbf{k}_{bj}|\omega\cosh(k_1h)}$$
$$\times\left[\sinh(|\mathbf{k}_1\pm\mathbf{k}_{bj}|\tilde{z}) + \cosh(|\mathbf{k}_1\pm\mathbf{k}_{bj}|\tilde{z})\beta(|\mathbf{k}_1\pm\mathbf{k}_{bj}|)\right], \tag{10a}$$

$$\beta(k) = \frac{\omega^2\tanh(kh) - gk}{gk\tanh(kh) - \omega^2} \tag{10b}$$

$$\mathscr{D}(z) = -\sinh(k_1\tilde{z})\frac{Agd_1\mathbf{k}_1\cdot\mathbf{k}_2}{4k_1\omega\cosh(k_1h)} \tag{10c}$$

$$\mathscr{E}(z) = \cosh(k_1\tilde{z})\frac{iAg^2d_1\mathbf{k}_1\cdot\mathbf{k}_2}{8\omega^2\cosh^3(k_1h)}. \tag{10d}$$

in which $\tilde{z} \equiv z + h$. From (9) it is seen that the amplitude of the resonant wave $\mathbf{k}_2 = \mathbf{k}_1 + \mathbf{k}_{b1}$ linearly increases with time. This is a direct result from Class I Bragg resonance. Note that here we keep non-growing terms in (9) as they will contribute to the resonance at the next (i.e. third) order. At the third order, the governing equations read

$$\nabla^2\phi_3 = 0, \ \text{ in } \ -h \le z \le 0, \tag{11a}$$
$$\phi_{3tt} + g\phi_{3z} = \text{N.R.}, \ \text{ on } \ z = 0, \tag{11b}$$
$$\phi_{3z} = \nabla_h\cdot(\zeta\nabla_h\phi_2) + \nabla_h\cdot(\frac{\zeta^2}{2}\nabla_h\phi_1), \ \text{ on } \ z = -h, \tag{11c}$$

whose solution has the form

$$\begin{aligned}\phi_3 =& \left(\mathscr{A}(z) + \mathscr{B}(z)t + \mathscr{C}(z)t^2\right)\mathrm{e}^{i(\mathbf{k}_1\cdot\mathbf{x}-\omega t)} +\\ &\left(\mathscr{F}(z) + \mathscr{G}(z)t + \mathscr{H}(z)t^2\right)\mathrm{e}^{i(\mathbf{k}_3\cdot\mathbf{x}-\omega t)}\\ &+ c.c. + \text{locked waves},\end{aligned} \tag{12}$$

where

$$\begin{aligned}\mathscr{A}(z) =& -\sinh(k_1\tilde{z})\left\{\frac{Ag(d_1^2+d_2^2)k_1}{8\omega\cosh(k_1h)} + \frac{d_1}{2k_1}\mathbf{k}_1\cdot\left[(\mathbf{k}_1-\mathbf{k}_{b1})\mathscr{K}_1^{-}(-h)\right.\right.\\ &\left.\left.+\mathbf{k}_2\mathscr{D}(-h) + \frac{d_2}{d_1}(\mathbf{k}_1\pm\mathbf{k}_{b2})\mathscr{K}_2^{\pm}(-h)\right]\right\},\\ \mathscr{B}(z) =& -\left[\sinh(k_1\tilde{z}) - \cosh(k_1\tilde{z})\frac{1+3\tanh^2(k_1h)}{4\tanh(k_1h)}\right]\\ &\frac{d_1\mathscr{E}(-h)\mathbf{k}_1\cdot\mathbf{k}_2}{2k_1} - \coth(k_1\tilde{z})\frac{igk_1\mathscr{A}(z)}{2\omega\cosh^2(k_1h)},\\ \mathscr{C}(z) =& \cosh(k_1\tilde{z})\frac{id_1g\mathscr{E}(-h)\mathbf{k}_1\cdot\mathbf{k}_2}{8\omega\cosh^2(k_1h)},\\ \mathscr{F}(z) =& -\sinh(k_1\tilde{z})\left[\frac{Agd_1d_2\mathbf{k}_1\cdot\mathbf{k}_3}{8k\omega\cosh(k_1h)} + \frac{d_2\mathscr{D}(-h)\mathbf{k}_2\cdot\mathbf{k}_3}{2k_1}\right],\\ \mathscr{G}(z) =& -\left[\sinh(k_1\tilde{z}) - \cosh(k_1\tilde{z})\frac{1+3\tanh^2(k_1h)}{4\tanh(k_1h)}\right]\\ &\frac{d_2\mathscr{E}(-h)\mathbf{k}_2\cdot\mathbf{k}_3}{2k_1} - \coth(k_1\tilde{z})\frac{ig\mathscr{F}}{2\omega\cosh^2(k_1h)},\\ \mathscr{H}(z) =& \cosh(k_1\tilde{z})\frac{id_2g\mathscr{E}(-h)\mathbf{k}_2\cdot\mathbf{k}_3}{8\omega\cosh^2(k_1h)},\end{aligned}$$

in which $\mathbf{k}_3 = \mathbf{k}_2 + \mathbf{k}_{b_2}$. The free-surface elevation associated with waves $\mathbf{k}_1, \mathbf{k}_2$ and $\mathbf{k}_3$ up to the third order is then given by

$$\begin{aligned}
\eta =& \eta_1 + \eta_2 + \eta_3 + \mathscr{O}(\varepsilon^4), \\
=& -\frac{\phi_{1t}}{g} - \frac{\phi_{2t}}{g} - \frac{\phi_{3t}}{g} + \text{locked waves} + \mathscr{O}(\varepsilon^4), \ \text{ on } \ z = 0, \\
=& \Big\{ \frac{iA}{2} + \frac{1}{g}\left[i\omega\mathscr{A}(0) - \mathscr{B}(0) + (i\omega\mathscr{B}(0) - 2\mathscr{C}(0))t \right. \\
& \left. + i\omega\mathscr{C}(0)t^2 \right] \Big\} \mathrm{e}^{i(\mathbf{k}_1\cdot\mathbf{x} - \omega t)} \\
& + \frac{1}{g}\left[i\omega\mathscr{D}(0) - \mathscr{E}(0) + i\omega\mathscr{E}(0)t \right] \mathrm{e}^{i(\mathbf{k}_2\cdot\mathbf{x} - \omega t)} \\
& + \frac{1}{g}\left[i\omega\mathscr{F}(0) - \mathscr{G}(0) + (i\omega\mathscr{G}(0) \right. \\
& \left. - 2\mathscr{H}(0))t + i\omega\mathscr{H}(0)t^2 \right] \mathrm{e}^{i(\mathbf{k}_3\cdot\mathbf{x} - \omega t)} + \mathscr{O}(\varepsilon^4).
\end{aligned} \tag{14}$$

It is clear that the growth of the intermediate wave (i.e. $\mathbf{k}_2$) is linear in time, as is expected from Class I Bragg resonance, while that of the third-order resonant wave $\mathbf{k}_3$ is quadratic in time. The decrease in amplitude of the incident wave $\mathbf{k}_1$ is, accordingly, also quadratic in time. The presented results of (14) are only valid for initial times and as long as $\eta_2 \ll \eta_1$ and $\eta_3 \ll \eta_2$. This also can be seen from an energy point of view as (14) shows an unbounded growth of η_2, η_3 with time that violates energy conservation.

In order to find the long-term rate of energy transfer between the shoreward incident wave and the shore-parallel resonant wave we adopt an analysis based on the multiple-scales method. We introduce slow variables $\bar{x}, \bar{y}, \bar{t} = \varepsilon x, \varepsilon y, \varepsilon t$ and assume that the solution $\Phi(\mathbf{x}, t, \bar{x}, \bar{y}, \bar{t})$ to the problem (1) can be expressed at all times in terms of a convergent series

$$\Phi = \varepsilon\phi_1 + \varepsilon^2\phi_2 + \ldots \tag{15}$$

in which $\phi_1, \phi_2 \sim \mathscr{O}(1)$ are functions of the original $(\mathbf{x}, t)$, and slow $(\bar{x}, \bar{y}, \bar{t})$ variables. Substituting the expansion (15) into (1) and collecting same order terms, governing equations at each order are obtained. For the solution of the leading order problem $\mathscr{O}(\varepsilon)$, since a simultaneous Class I and II Bragg resonance are expected, we consider three free propagating waves on the surface with the potential

$$\begin{aligned}
\phi_1 &= \sum_{j=1}^{3} \alpha_j(z; \bar{x}, \bar{y}, \bar{t})\ \mathrm{e}^{i(\mathbf{k}_j\cdot\mathbf{x} - \omega t)} + c.c., \\
\alpha_j(z; \bar{x}, \bar{y}, \bar{t}) &\equiv A_j(\bar{x}, \bar{y}, \bar{t})\ \frac{g}{2\omega}\ \frac{\cosh[k_1(z+h)]}{\cosh(k_1 h)},
\end{aligned} \tag{16}$$

where j=1,2,3 refer to the waves with wavenumber $\mathbf{k}_1, \mathbf{k}_2$ and $\mathbf{k}_3$ respectively. At the second order $\mathscr{O}(\varepsilon^2)$, the governing equations read

$$\nabla^2\phi_2 + 2\bar{\nabla}\cdot\nabla\phi_1 = 0, \ \text{ in } \ -h \le z \le 0, \tag{17a}$$
$$\phi_{2,tt} + g\phi_{2,z} + 2\phi_{1,t\bar{t}} = \text{N.R.}, \ \text{ on } \ z = 0, \tag{17b}$$
$$\phi_{2,z} = \nabla_h\cdot(\zeta\nabla_h\phi_1), \ \text{ on } \ z = -h, \tag{17c}$$

where $\bar{\nabla} = (\partial_{\bar{x}}, \partial_{\bar{y}})$. We assume that the second order potential ϕ_2 has the form

$$\phi_2 = \sum_{j=1}^{3} \psi_j(z)\mathrm{e}^{i(\mathbf{k}_j\cdot\mathbf{x} - \omega t)} + c.c., \tag{18}$$

that upon substitution in (17) gives the following equations for the ψ_j's (j =1,2,3)

$$\psi_{j,zz} - k_1^2\psi_j = -2\mathrm{i}\frac{g\cosh[k_1(z+h)]}{2\omega\cosh(k_1 h)}\bar{\nabla}\cdot(\mathbf{k}_j A_j), \ \text{ in } \ -h \le z \le 0, \tag{19a}$$
$$-\omega^2\psi_j + g\psi_{j,z} = igA_{j,\bar{t}} + \text{N.R.}, \ \text{ on } \ z = 0, \tag{19b}$$
$$\psi_{j,z} = \gamma_{jm}\frac{gA_m}{2\omega\cosh(k_1 h)}, \ \text{ on } \ z = -h, \tag{19c}$$

with $\gamma_{11} = \gamma_{13} = \gamma_{22} = \gamma_{31} = \gamma_{33} = 0$, and $\gamma_{12} = \gamma_{21} = -(d_1/2)\,\mathbf{k}_1\cdot\mathbf{k}_2, \gamma_{23} = \gamma_{32} = -(d_2/2)\,\mathbf{k}_2\cdot\mathbf{k}_3$. Note that the α_j's (c.f. (16)) are homogeneous solutions of (19). Therefore, the system (19) admits non-trivial solutions ψ_j if and only if the so-called compatibility condition is satisfied [29]. Applying Green's second identity, and denoting complex conjugates by an asterisk, the solvability condition can be cast into

$$\int_{-h}^{0} dz\left[\alpha_j^*(\psi_{j,zz} - k_1^2\psi_j) - \psi_j(\alpha_{j,zz}^* - k_1^2\alpha_j^*)\right] = \left[\alpha_j^*\frac{\partial\psi_j}{\partial z} - \psi_j\frac{\partial\alpha_j^*}{\partial z}\right]_{-h}^{0} \tag{20}$$

which, after some manipulations, reduces to a system of coupled partial-differential equations for the slowly varying wave envelopes, i.e.,

$$\frac{\partial}{\partial\bar{t}}\left(\frac{|A_j|^2}{2}\right) + \bar{\nabla}\cdot\left(\mathbf{C}_{\mathbf{g}_j}\frac{|A_j|^2}{2}\right) = iA_j^*\begin{cases} A_2\Omega_1, & j = 1 \\ A_1\Omega_1 + A_3\Omega_3, & j = 2 \\ A_2\Omega_3, & j = 3 \end{cases} \tag{21}$$

with

$$\Omega_1 = \frac{\omega d_1 \mathbf{k}_1 \cdot \mathbf{k}_2}{2k_1 \sinh(2k_1 h)}, \tag{22a}$$

$$\Omega_3 = \frac{\omega d_2 \mathbf{k}_2 \cdot \mathbf{k}_3}{2k_1 \sinh(2k_1 h)}, \tag{22b}$$

$$\mathbf{C}_{\mathbf{g}_j} = \frac{\mathbf{k}_j \omega}{2k_1^2}\left[1 + \frac{2k_1 h}{\sinh(2k_1 h)}\right] = \frac{\mathbf{k}_j}{k_1} C_g. \tag{22c}$$

Adding the partial-differential equation for A_2 to the complex conjugate of those of A_1, A_3 we obtain the well-known conservation law of wave action, i.e.

$$\frac{\partial}{\partial \bar{t}}\left(\frac{|A_1|^2}{2} + \frac{|A_2|^2}{2} + \frac{|A_3|^2}{2}\right) + \bar{\nabla}\cdot\left(\mathbf{C}_{\mathbf{g}_1}\frac{|A_1|^2}{2} + \mathbf{C}_{\mathbf{g}_2}\frac{|A_2|^2}{2} + \mathbf{C}_{\mathbf{g}_3}\frac{|A_3|^2}{2}\right) = 0. \tag{23}$$

Equation (21) can also be simplified into the following form

$$\frac{\partial}{\partial \bar{t}} A_j + \bar{\nabla}\cdot\left(\mathbf{C}_{\mathbf{g}_j} A_j\right) = i\begin{cases} A_2\Omega_1, & j=1 \\ A_1\Omega_1 + A_3\Omega_3, & j=2 \\ A_2\Omega_3, & j=3 \end{cases} \tag{24}$$

which can be readily shown to reduce to equations (2.33)-(2.34) of [13] for a single bottom corrugation ($d_2 = 0$).

If the patch of bottom ripples is infinitely large and initial condition is spatially uniform then everything must remain uniform in space, i.e. all spatial variations vanish. In that case we have

$$\frac{\partial}{\partial \bar{t}}\begin{Bmatrix} A_1 \\ A_2 \\ A_3 \end{Bmatrix} = i\begin{bmatrix} 0 & \Omega_1 & 0 \\ \Omega_1 & 0 & \Omega_3 \\ 0 & \Omega_3 & 0 \end{bmatrix}\begin{Bmatrix} A_1 \\ A_2 \\ A_3 \end{Bmatrix}, \tag{25}$$

which admits the solution

$$\begin{Bmatrix} A_1 \\ A_2 \\ A_3 \end{Bmatrix} = c_0\begin{Bmatrix} -\Omega_3/\Omega_1 \\ 0 \\ 1 \end{Bmatrix} + c_+\begin{Bmatrix} \Omega_1/\Omega_3 \\ \sqrt{\Omega_1^2+\Omega_3^2}/\Omega_3 \\ 1 \end{Bmatrix} e^{i\Omega_0 t_1} + c_-\begin{Bmatrix} \Omega_1/\Omega_3 \\ -\sqrt{\Omega_1^2+\Omega_3^2}/\Omega_3 \\ 1 \end{Bmatrix} e^{-i\Omega_0 t_1}, \tag{26}$$

where $\Omega_0 = \sqrt{\Omega_1^2+\Omega_3^2}$. The coefficients $c_0,\ c_+,\ c_-$ are to be determined from the initial condition.

The special case of our main interest is when a free propagating surface wave $\mathbf{k}_1$ with initial amplitude $A = -ia_0$ propagates over an infinite patch of doubly-sinusoidal corrugations. We assume that the topography wavenumbers $\mathbf{k}_{b_1}, \mathbf{k}_{b_2}$ are chosen such that wave $\mathbf{k}_2$ makes an angle θ with $\mathbf{k}_1$, and wave $\mathbf{k}_3$ is perpendicular to $\mathbf{k}_1$ as shown in figure 1. From equation (26) we obtain

$$\begin{Bmatrix} A_1 \\ A_2 \\ A_3 \end{Bmatrix} = -ia_0\begin{Bmatrix} \sin^2\theta + \cos^2\theta\cos(\Omega_0\bar{t}) \\ -i\cos\theta\sin(\Omega_0\bar{t}) \\ \sin\theta\cos\theta[-1+\cos(\Omega_0\bar{t})] \end{Bmatrix}. \tag{27}$$

Variations of the normalized amplitudes $\hat{a}_j = |A_j/a_0|$ as a function of $\bar{t}/T$ where $T = 2\pi/\omega$ is shown in figure 2a-c for respectively three angles $\theta = \pi/8, \pi/4$ and $3\pi/8$. For $\theta = \pi/8$ (figure 2a) the amplitude of the wave $\mathbf{k}_1$ becomes zero at times, but at those times energy is partitioned between waves $\mathbf{k}_2, \mathbf{k}_3$ and in fact wave $\mathbf{k}_2$ holds a larger portion of the energy. As θ grows, the maximum of amplitude of $\hat{a}_3$ also grows until at $\theta = \pi/4$ it reaches its maximum of $\hat{a}_3$=1. At that moment, $\hat{a}_1, \hat{a}_2$=0 (as expected from the energy conservation) and therefore all the energy of the incident wave $\mathbf{k}_1$ is now transferred to the wave $\mathbf{k}_3$. As θ further increases from $\pi/4$ the amplitude of the incident wave $\hat{a}_1$ can no longer reach zero in any time, and likewise $\hat{a}_3$ can no longer reach unity. Clearly the optimum case is at $\theta = \pi/4$ for which all the energy of the shoreward incident wave $\mathbf{k}_1$ can be transferred to a shore-parallel wave $\mathbf{k}_3$.

Direct Simulation

A realistic consideration of a patch of seabed bars for coastal protection must take into account all resonance and near-resonance interactions as well as the effect of the finiteness of the patch and boundaries. As a general approach to address these, here we use a direct simulation scheme of high-order spectral method. The scheme solves the potential flow equation (1) assuming the solution can be expressed in terms of a convergence series [30]. It can take up to an arbitrary order of nonlinearity M (i.e. number of terms in the perturbation expansion, typically $M \sim \mathscr{O}(10)$) and a high number of wave modes N (typically $N \sim \mathscr{O}(10,000)$. The method was first formulated by [31] and [32] to model nonlinear wave-wave interactions in deep water. It was then extended to the problems of wave-topography interactions in finite depth [6, 21, 33] and two-layer density stratified fluids [34–38] as well as wave viscoelastic-seabed interactions [39]. The scheme has already undergone extensive convergence tests as well as validations against experimental and other numerical results [39–42].

For the cross validation of the direct simulation results with those of analytical (regular perturbation and multiple scales), we consider a case of an incident wave traveling over a doubly-

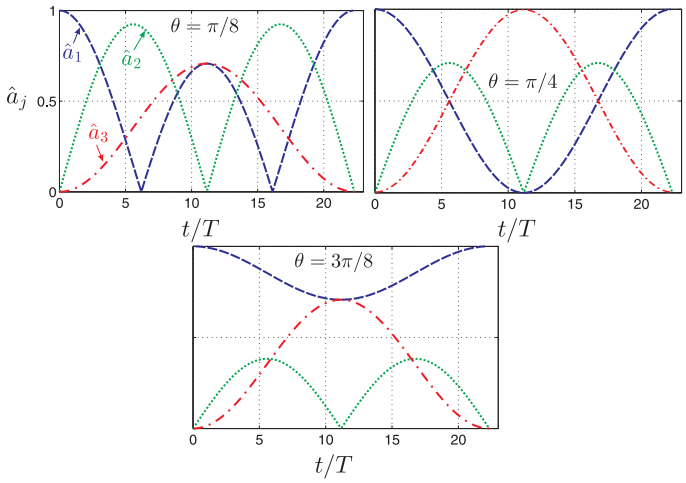

FIGURE 2: Time evolution of the normalized amplitude envelopes of the $\mathbf{k}_1, \mathbf{k}_2$ and $\mathbf{k}_3$ waves, respectively shown by blue dashed lines ($\hat{a}_1$), green dotted lines ($\hat{a}_2$) and red dash-dotted lines ($\hat{a}_3$) for three resonance angles $\theta = \pi/8, \pi/4$ and $3\pi/8$ (c.f. figure 1). The objective for shore protection is to divert as much energy as possible from the shore-normal incident wave $\mathbf{k}_1$ to the shore-parallel reflected wave $\mathbf{k}_3$. Clearly this objective is best met for $\theta = \pi/4$ in which a diversion efficiency of 100% is achieved.

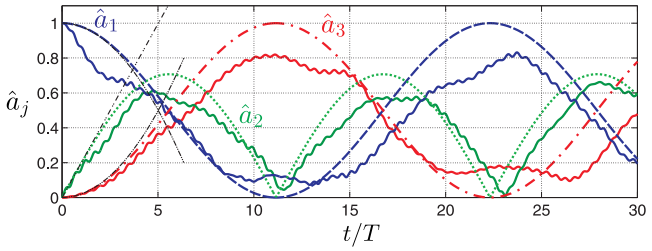

FIGURE 3: Comparison of amplitude envelopes of three waves $\mathbf{k}_1, \mathbf{k}_2, \mathbf{k}_3$ engaged in a special case of Class II Bragg resonance in which $\mathbf{k}_1, \mathbf{k}_2$ satisfy a Class I Bragg resonance condition with one of the bottom components. As a result of such resonance, amplitude of the wave $\mathbf{k}_3$ increases quadratically with time and much faster than classical Class II resonance. Plotted are normalized amplitudes envelopes $\hat{a}_1, \hat{a}_2$ and $\hat{a}_3$ as predicted by regular perturbation (black dash-double-dotted line), multiple scales analysis (dotted, dashed and dash-dotted lines), and direct simulation (solid lines). All three approaches agree relatively well for the initial time of the simulation, but regular perturbation deviates from the other two for longer times. Multiple scales and direction simulation predictions stay in a good proximity.

periodic topography in a square area with periodic boundary conditions. In our computations we assume that the length scale L_0 is chosen such that the physical domain is mapped to the simulation domain of $x, y \in [0 \;\; 2\pi)$, and the time scale T_0 is chosen according to $T_0 = \sqrt{L_0/g}$. In the dimensionless simulation domain we pick $\mathbf{k}_1 = 41\hat{i}$, and other variables are chosen such that $k_1 h$=0.41, $\varepsilon_s = k_1 a$=0.041. For the seabed bars $\theta = \pi/4$ (c.f. figure 1), such that $k_{b1} = k_{b2}$=31.38, and $\varepsilon_b = k_{1b} a_b$=0.063. Simulations parameters are $N_x = N_y = 1024$, $M = 4$ and $T/\delta t = 16$ for which results are converged.

Results of direct simulation of this case as a function of normalized time (t/T) are shown in figure 3 (solide lines) and compared with results of regular perturbation (dash-double dotted black lines) and multiple scales (dashed, dash-dotted and dotted lines). Note that the initial growth rates predicted by regular perturbation (14) can be readily shown to match, at the leading order, with those obtained from the Taylor expansion of the multiple scales solution (27) near t=0, that are

$$\begin{Bmatrix} \hat{a}_1 \\ \hat{a}_2 \\ \hat{a}_3 \end{Bmatrix} \sim \begin{Bmatrix} 1 - \Omega_0^2 t^2/4 \\ \frac{1}{\sqrt{2}}\Omega_0 t \\ \Omega_0^2 t^2/4 \end{Bmatrix} = \begin{Bmatrix} |1 + \frac{\omega}{g}\mathscr{C}(0)t^2| \\ |\frac{\omega}{g}\mathscr{E}(0)t| \\ |\frac{\omega}{g}\mathscr{H}(0)t^2| \end{Bmatrix} / (\frac{a_0}{2}), \quad (28)$$

which corresponds to a quadratic decay, linear growth, and quadratic growth of the wave amplitudes $\hat{a}_1, \hat{a}_2$ and $\hat{a}_3$ respectively. For the growth rate of amplitudes $\hat{a}_2, \hat{a}_3$, as is seen in figure 3, regular perturbation, multiple scales and direct simulation match very well during the initial stage of the interaction ($0 < t/T < 2$). But then direct simulation and multiple scales results deviate from those of regular perturbation. This is expected as beyond the initial stage of the interaction the underlying assumption of regular perturbation does not hold resulting in prediction of indefinite growth in the amplitude over time which is clearly non-physical. Multiple scales and direct simulation, however, show a satisfactory agreement with each other over a very long time. The discrepancy evidently comes from energy spreading to non-resonant and near-resonant modes [33]. This is highlighted in the sudden drop of amplitude of $\hat{a}_1$ whose loss of energy apparently does not go to any of waves $\hat{a}_2$ and/or $\hat{a}_3$. Note that multiple scales results are energy conserving. Therefore when the increase in the amplitude of $\hat{a}_2, \hat{a}_3$ is the same in the direct simulation and multiple-scales, the energy associated with the excess of drop in the amplitude of $\hat{a}_1$ in direct simulation has to go to other (locked and/or free) modes rather than $\hat{a}_2$ and $\hat{a}_3$.

For the direct simulation of sheltering, we will first consider wave attenuation downstream of a finite patch of doubly-sinusoidal bars incident on an absorbing shoreline, and then investigate the effect of the shoreline reflection. In our computations we choose the same normalization as in the validation case with $\mathbf{k}_1 = 128\hat{i}$, $k_1 h$=0.31, $\varepsilon_s = k_1 a$=0.011, and for the seabed bars $\theta = \pi/4$ (that results in $k_{b1} = k_{b2}$=97.967), and

$\varepsilon_b = k_{1b}a_b$=0.030. Simulations parameters are chosen the same as before. We define a Cartesian coordinate system with its origin at the center of the computational domain. For the ease of presentation, we define variables in this coordinate system (x,y) as the horizontal variables in the computational domain (that are already dimensionless) normalized by the wavelength of the incident wave $\lambda_1 = 2\pi/k_1$. Therefore every single spatial unit in the following figures correspond to one wavelength of the incident wave. In this coordinate system, $x = 0$ denotes the shoreline. We consider a finite patch of doubly-sinusoidal topography ($\theta = \pi/4$, c.f. figure 1) that occupies $23 < x < 35$, that is, the horizontal extent of the patch in the x-direction is $12\lambda_1$. This patch length is expected to be large enough for a good part of energy of incoming waves to be redirected, since multiple scales results predict that over a uniform infinite topography, a distance of $C_g \frac{2\pi}{\Omega_0} \sim 14\lambda_1$ is required for a perfect sheltering. We also consider that the patch is symmetric about $y = 0$ axis, but long in the y-direction. Incident waves are created by a numerical wavemaker (that also absorbs reflected waves) near $x \sim 60$ and propagate forward toward the shore ($x = 0$). A numerical wave absorber is implemented at the end of the computational domain ($x/\lambda_1 \sim -64$) so that waves do not reflect back.

Energy and the momentum that shoreline receives are functions of the shoreward wave energy flux. A more conservative and more insightful measure is spatial distribution of the time-average wave-energy density. We define the normalized average energy density as

$$\bar{E}(x,y) = \frac{\int_{t_0}^{t_f} \eta(x,y)^2 \, \mathrm{d}t}{\int_{t_0}^{t_f} \eta_0(x,y)^2 \, \mathrm{d}t} \tag{29}$$

where here we choose $t_f = t_0 + 40T$ in which t_0 is an arbitrary time *after* the steady-state is reached, and η_0 is the water surface in the absence of the topography (i.e. with just a free propagating wave with the wavenumber $\mathbf{k}_1$). The integral in the denominator is obtained by running a simulation over a flat bottom. Normalized energy density $\bar{E}$ obtained from the direct simulation of the above case is shown in figure 4a. Normal to the shore waves enter from $x = +\infty$ and, upon interaction with the patch of bars are pushed side-ways creating a buffer zone downstream where energy activity is minimum (almost zero). Since the patch is intentionally designed sub-optimum and also because of discontinuity of the patch at $y = 0$ two beams of wave $\mathbf{k}_2$ scape the patch and propagate shoreward, but do not interfere with the protected buffered area. Since the spatial distribution of $\bar{E}$ has a very fine structure, for a better presentation purpose, we also show the spatial average of $\bar{E}$ calculated over areas of $2\lambda_1 \times 2\lambda_1$, i.e. $\bar{\bar{E}} = (1/4\lambda_1^2) \int_{x_0}^{x_0+2\lambda_1} \int_{y_0}^{y_0+2\lambda_1} \bar{E} \, \mathrm{d}x \, \mathrm{d}y$ (see figure 4.b). This figure in fact confirms the shielded area, and also shows that the two beams of $\mathbf{k}_2$ carry just a little more energy that the case of only incident wave: beams of $\mathbf{k}_2$ hit the shoreline at $y \sim \pm 40$ with an amplitude slightly greater than unity apparent from the yellowish color in figure 4b. The area right above the patch ($23 < x < 35$) is in fact very energetic.

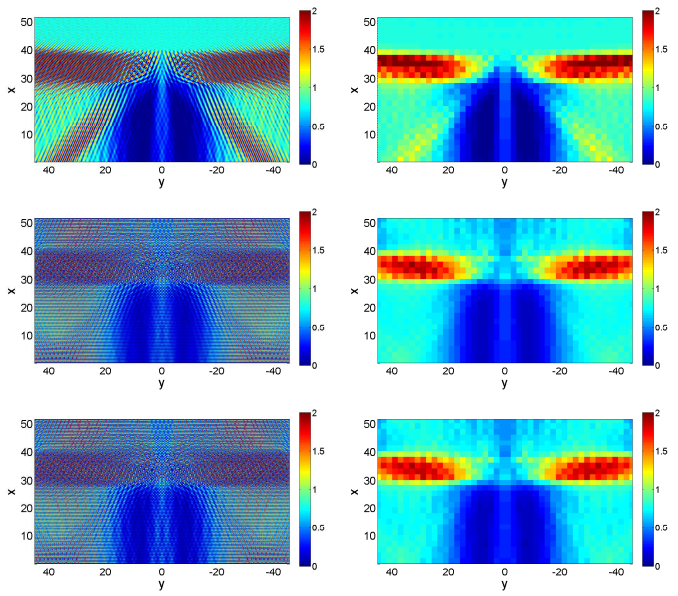

FIGURE 4: (a). Spatial distribution of the normalized average energy density $\bar{E}$ for a patch of doubly sinusoidal oblique bars placed in the area $23 < x < 35$, symmetric about $y = 0$, and with $\theta = \pi/4$. The beach ($x = 0$) is perfectly absorbing. Incident waves $\mathbf{k}_1$ arriving from $x = +\infty$ are diverted sideways to the wave $\mathbf{k}_3$ by the patch of ripples through intermediate wave $\mathbf{k}_2$. Two beams of wave $\mathbf{k}_2$ are seen leaving the patch with angle $\pi/4$ with respect to the patch and hit the shoreline at $y \sim \pm 40$. Wave activity in the area $y = \pm 20$ is almost zero, and hence a protected shore is achieved. (b) Plot of $\bar{\bar{E}}$ the spatial average of $\bar{E}$ over blocks of $2\lambda_1 \times 2\lambda_1$. (c,d) Plots of $\bar{E}$ and $\bar{\bar{E}}$ similar to the case (a,b) but with a perfectly reflecting beach at $x = 0$. (e,f) an example of insensitivity of the proposed scheme to the shoreline-patch distance. The figure is the same case of (c,d) but with shoreline-patch distance reduced with $\lambda_1/8$. Clearly no qualitative and graphically-distinguishable quantitative difference is observed (c.f. the case of normal Bragg protection where the same change in the distance results in several times higher/lower wave amplitude at the shoreline as shown by [1]).

The most important point raised by [1], supported by experimental observations and numerical studies [25,43,44], is that the protection of a finite reflecting shore via normal Bragg resonance is sensitive to the distance d of the bars strip to the shoreline. Specifically, for some distances the amplitude of the wave grows toward the shore. While physically speaking this should not be of any concern to the approach presented here, for completeness we computationally investigate the sensitivity of the proposed shore

protection scheme to the shoreline-patch distance. For this purpose, we consider the case of a perfectly *reflecting* beach. All the physical and simulations parameters are the same as the case of a perfectly *absorbing* beach, with the exception of the shoreline being reflective. In the absence of the topography, standing waves with amplitude $2a_0$ will be formed on the water surface. Similar to the case of a perfectly absorbing beach, we calculate the denominator of (29) from an independent simulation without the presence of the patch of bottom ripples. Results of $\bar{E}$ and $\bar{\bar{E}}$ are shown in figures 4c,d. A very good protection is obtained in this case as well. The upstream of the patch from figure 4c seems to be energetic, but on avarge it has the same energy as in the absence of the patch (and not more, c.f. figure 4d). The $\mathbf{k}_2$ beams are also clearly seen here to hit the shoreline and reflect back with an angle $\pi/4$ (more clear in figure 4c). The trends are very similar to that of a perfectly absorbing beach.

ACKNOWLEDGMENTS

This publication was made possible, in part, with the support from the National Science Foundation (Grant No. CBET-1414579-EAGER), the American Bureau of Shipping, and the U.C. Berkeley Committee on Research.

CONCLUSIONS

Long crested periodic seabed bars known to reflect incident ocean waves of double the wavelength via engaging them in the so called Bragg resonance. Such seabed bars are, however, known to be unable to protect the shore as the shielding efficiency is very much sensitive to the distance of the shoreline to the patch of the bars. Small variations in this distance may result in wave amplitudes much larger than the amplitude in the absence of the protecting bars. Here, we propose an arrangement of seabed bars that based on oblique Bragg resonance diverts the incident wave sideways. We show that this configuration is insensitive to the shoreline-patch distance and can efficiently shield the shore.

Sheltering by an array of longshore bars gradually divert the incoming wave energy while posing much less stress on the seabed (compared to, for instance, breakwaters). It is more reliable (no sudden breakdown), and cost effective (since it is seabed based, hence no major foundation), and is environmentally friendly. The proposed idea may also be used to protect nearshore shallow water important infrastructures (e.g. offshore wind farms) susceptible and vulnerable to cyclic wave loads. Our proposed sheltering idea can sit on the seabed providing a uniform reflection of the water waves with a fraction of the cost and environmental impact of the seawalls (also c.f. [45]). Our sheltering idea can also provide a calm water habitat for marine life reproduction hence supporting fisheries.

REFERENCES

[1] Yu, J., and Mei, C. C., 2000. "Do longshore bars shelter the shore?". *Journal of Fluid Mechanics,* ***404***, pp. 251–268.

[2] Davies, A. G., and Heathershaw, A. D., 1984. "Surface-wave propagation over sinusoidally varying topography". *J. Fluid Mechanics,* ***144***, pp. 419–443.

[3] Mei, C. C., Hara, T., and Naciri, M., 1988. "Note on Bragg scattering of water waves by parallel bars on the seabed". *Journal of Fluid Mechanics,* ***186***, pp. 147–162.

[4] Ardhuin, F., and Herbers, T. H. C., 2002. "Bragg scattering of random surface gravity waves by irregular seabed topography". *J. Fluid Mech.,* ***451***, pp. 1–33.

[5] Madsen, P. A., and Fuhrman, D. R., 2006. "Third-order theory for bichromatic bi-directional water waves". *J. Fluid Mech.,* ***557***, pp. 369–397.

[6] Liu, P. L.-F., Yeh, H., Lin, P., Chang, K.-T., and Cho, Y.-S., 1998. "Generation and evolution of edge-wave packets". *Physics of Fluids,* ***10***(7), p. 1635.

[7] Pinsker, Z. G., 1978. *Dynamical Scattering of X-rays in Crystals*, Vol. 3. Springer-Verlag Berlin.

[8] Alam, M.-R., and Mei, C. C., 2007. "Attenuation of long interfacial waves over a randomly rough seabed". *Journal of Fluid Mechanics,* ***587***, pp. 73–96.

[9] Alam, M.-R., and Mei, C. C., 2008. "Ships advancing near the critical speed in a shallow channel with a randomly uneven bed". *Journal of Fluid Mechanics,* ***616***, pp. 397–417.

[10] Davies, A., 1982. "The reflection of wave energy by undulations on the seabed". *Dynamics of Atmospheres and Oceans,* ***6***, pp. 207–232.

[11] Heathershaw, A., 1982. "Seabed-wave resonance and sand bar growth". *Nature,* ***296***(25), pp. 343–345.

[12] Mitra, A., and Greenberg, M., 1984. "Slow Interactions of Gravity Waves and a Corrugated Sea Bed". *Journal of Applied Mechanics,* ***51***(251), pp. 5–9.

[13] Mei, C. C., 1985. "Resonant reflection of surface water waves by periodic sandbars". *Journal of Fluid Mechanics,* ***152***, pp. 315–335.

[14] Kirby, J. T., 1986. "A general wave equation for waves over rippled beds". *J. Fluid Mech.,* ***162***, pp. 171–186.

[15] Porter, R., and Porter, D., 2001. "Interaction of water waves with three-dimensional periodic topography". *J. Fluid Mechanics,* ***434***, pp. 301–335.

[16] Liu, Y., and Yue, D. K.-P., 1998. "On generalized Bragg scattering of surface waves by bottom ripples". *Journal of Fluid Mechanics,* ***356***, pp. 297–326.

[17] Elgar, S., Raubenheimer, B., and Herbers, T. H. C., 2003. "Bragg reflection of ocean waves from sandbars". *Geophys. Res. Lett.,* ***30***.

[18] Hara, T., and Mei, C. C., 1987. "Bragg scattering of surface waves by periodic bars: theory and experiment". *Journal of Fluid Mechanics,* ***178***(-1), Apr., pp. 221–241.

[19] Elandt, R. B., Couston, L.-A., Lambert, R. A., and Alam,

M.-R., 2015. “Bragg resonance of gravity waves and ocean renewable energy”. In *Integrated Systems: Innovations and Applications*. Springer, pp. 211–225.

[20] Guazzelli, E., Rey, V., and Belzons, M., 1991. “Higher-order Bragg reflection of gravity surface waves by periodic beds”. *Journal of Fluid Mechanics Digital Archive,* ***245***(-1), pp. 301–317.

[21] Alam, M.-R., Liu, Y., and Yue, D. K., 2010. “Oblique sub-and super-harmonic bragg resonance of surface waves by bottom ripples”. *Journal of Fluid Mechanics,* ***643***, pp. 437–447.

[22] Baillard, J., DeVries, J., Kirby, J. T., and Guza, R. T., 1990. “Bragg Reflection Breakwater: A New Shore Protection Method?”. In Coastal Engineering Proceedings, pp. 1702–1715.

[23] Baillard, J. A., Devries, J. W., and Kirby, J. T., 1992. “Considerations in using Bragg reflection for storm erosion protection”. *Journal of Waterway, Port, Coastal, and Ocean Engineering,* ***118***(1), pp. 62–74.

[24] Couston, L.-A., Guo, Q., Chamanzar, M., and Alam, M.-R., 2015. “Fabry-perot resonance of water waves”. *Physical Review E,* ***92***(4), p. 043015.

[25] Kirby, J. T., and Anton, J. P., 1990. “Bragg reflection of waves by artificial bars”. In Coastal Engineering Proceedings, no. 1, pp. 757–768.

[26] Howard, L. N., and Yu, J., 2007. “Normal modes of a rectangular tank with corrugated bottom”. *Journal of Fluid Mechanics,* ***593***, Nov., pp. 209–234.

[27] Liang, Y., and Alam, M.-R., 2014. “Asymmetric flexural-gravity lumps in nonuniform media”. *Physics of Fluids (1994-present),* ***26***(9), p. 092105.

[28] Guazzelli, E., Rey, V., and Belzons, M., 1992. “Higher-order Bragg reflection of gravity surface waves by periodic beds”. *Journal of Fluid Mechanics,* ***245***, p. 301.

[29] Fredholm, I., 1903. “Sur une classe déquations fonctionnelles”. *Acta Mathematica,* ***27***(1), pp. 365–390.

[30] Zakharov, V. E., 1968. “Stability of Periodic Waves of Finite Amplitude on the Surface of Deep Fluid”. *J. Appl. Mech. Tech. Phys.,* ***9***(2), pp. 190–194.

[31] Dommermuth, D. G., and Yue, D. K. P., 1987. “A high-order spectral method for the study of nonlinear gravity waves”. *Journal of Fluid Mechanics,* ***184***(-1), Apr., pp. 267–288.

[32] West, B., Brueckner, K., Janda, R., Milder, D., and Milton, R., 1987. “A new numerical method for surface hydrodynamics”. *Journal of Geophysical Research,* ***92***(C11), pp. 11803–11.

[33] Alam, M.-R., Liu, Y., and Yue, D. K., 2011. “Attenuation of short surface waves by the sea floor via nonlinear subharmonic interaction”. *Journal of Fluid Mechanics,* ***689***, pp. 529–540.

[34] Alam, M.-R., Liu, Y., and Yue, D. K., 2009. “Bragg resonance of waves in a two-layer fluid propagating over bottom ripples. part i. perturbation analysis”. *Journal of Fluid Mechanics,* ***624***, pp. 191–224.

[35] Alam, M.-R., Liu, Y., and Yue, D. K., 2009. “Bragg resonance of waves in a two-layer fluid propagating over bottom ripples. part ii. numerical simulation”. *Journal of Fluid Mechanics,* ***624***, pp. 225–253.

[36] Alam, M.-R., Liu, Y., and Yue, D. K., 2009. “Waves due to an oscillating and translating disturbance in a two-layer density-stratified fluid”. *Journal of Engineering Mathematics,* ***65***(2), pp. 179–200.

[37] Alam, M.-R., Liu, Y., and Yue, D. K., 2011. “Resonant-wave signature of an oscillating and translating disturbance in a two-layer density stratified fluid”. *Journal of Fluid Mechanics,* ***675***, pp. 477–494.

[38] Alam, M.-R., 2012. “Broadband cloaking in stratified seas”. *Physical review letters,* ***108***(8), p. 084502.

[39] Alam, M.-R., 2012. “Nonlinear analysis of an actuated seafloor-mounted carpet for a high-performance wave energy extraction”. *Proceedings of the Royal Society of London A: Mathematical, Physical and Engineering Sciences,* ***468***(2146), pp. 3153–3171.

[40] Toffoli, a., Gramstad, O., Trulsen, K., Monbaliu, J., Bitner-Gregersen, E., and Onorato, M., 2010. “Evolution of weakly nonlinear random directional waves: laboratory experiments and numerical simulations”. *Journal of Fluid Mechanics,* ***664***, Oct., pp. 313–336.

[41] Alam, M.-R., 2012. “A new triad resonance between co-propagating surface and interfacial waves”. *Journal of Fluid Mechanics,* ***691***, pp. 267–278.

[42] Alam, M.-R., 2014. “Predictability horizon of oceanic rogue waves”. *Geophysical Research Letters,* ***41***(23), pp. 8477–8485.

[43] O’Hare, T., and Davies, A., 1993. “Sand bar evolution beneath partially-standing waves: laboratory experiments and model simulations”. *Continental Shelf Research,* ***13***(11), Nov., pp. 1149–1181.

[44] Benjamin, T. B., Boczar-Karakiewicz, B., and Pritchard, W. G., 1987. “Reflection of water waves in a channel with corrugated bed”. *Journal of Fluid Mechanics,* ***185***(-1), Apr., p. 249.

[45] Zareei, A., and Alam, M.-R., 2015. “Cloaking in shallow-water waves via nonlinear medium transformation”. *Journal of Fluid Mechanics,* ***778***, pp. 273–287.